International Journal of Biological Macromolecules 81 (2015) 838–846

Contents lists available at ScienceDirect

International Journal of Biological Macromolecules

journal homepage: www.elsevier.com/locate/ijbiomac

A new porous magnetic chitosan modified by melamine for fast and efficient adsorption of Cu(II) ions

Zhan-Chao Wu*, Zhao-Zhan Wang, Jie Liu, Jin-Hua Yin, Shao-Ping Kuang*

State Key Laboratory Base of Eco-Chemical Engineering, Laboratory of Inorganic Synthesis and Applied Chemistry, College of Chemistry and Molecular Engineering, Qingdao University of Science and Technology, Qingdao 266042, PR China

ARTICLE INFO

Article history:
Received 3 June 2015
Received in revised form 29 July 2015
Accepted 13 September 2015
Available online 15 September 2015

Keywords:
Magnetic chitosan
Melamine
Adsorption of Cu(II)

ABSTRACT

A new porous magnetic chitosan modified by melamine (MA-CS/Fe_3O_4) was synthesized. The compositions and surface topographies were characterized by infrared (IR) spectroscopy, X-ray diffraction (XRD) analysis, thermogravimetric (TG) analysis and scanning electron microscope (SEM), respectively. The results of adsorption kinetics showed the adsorption behavior could be better described by the pseudo-second-order equation ($R > 0.999$). The adsorption isotherm was well fitted by the Langmuir equation ($R > 0.999$), and the values of separation factors were in the range of 0–1.0. The maximum adsorption capacity for Cu(II) was 2.58 mmol g^{-1} at the optimal experimental conditions, which were pH = 5.5, $t = 25$ min, $C_0 = 5.0$ mmol L^{-1}. The rate-controlling step was supposed to be chemical adsorption rather than mass transport. The adsorbent still exhibited high adsorption capacity after five regeneration cycles. The adsorption mechanism was due to coordination between Cu(II) and N atoms.

1. Introduction

Recently, water pollution caused by heavy metals has become serious environmental problem and attracted global attention [1]. Trace amounts of heavy metal ions cause serious pollution problem because of their high toxicity and non-biodegradability. So removal of toxic metal ions from wastewater is a subject of paramount importance [2,3]. Among these heavy metals, Cu(II) is the most common one, which is abundant in waste streams from copper electroplating and textile industries. According to the specification released by the U.S. Environmental Protection Agency (EPA), the maximum contaminant level (MCL) for Cu(II) is 1.3 mg L^{-1} in industrial effluents [4].

At present, there are several techniques for removing Cu(II) from wastewater, such as chemical precipitation, ion exchange, electrochemical separation process and adsorption technique [5]. Among them, the adsorption process using choitosan (CS) as adsorbent is one of the research hotspots due to the advantages of easy operation, and low cost [6].

CS derives from chitin, which are abundant, biodegradable, and renewable resources [7–10]. CS macromolecules are rich in amino and hydroxyl groups, which show high reaction activity with heavy metal ions and some organic compounds. Therefore, CS can be used as heavy metal ions adsorbents [11,12]. However, CS is unstable and easily soluble in acidic solutions. In addition, the adsorption capacity of CS for heavy metal ions is still insufficient due to the limited adsorption sites. All of these problems are stumbling blocks in the practical treatment of heavy metal ions [13,14]. So it is necessary for modifying CS in order to improve performance of adsorption and acid resistance. Generally, modifier compounds with high content of nitrogen, oxygen or sulfur are preferred to improve adsorption capability of CS, such as triethylene-tetramine (TETA) [15], ethanediamine [16], thiol [17–19], and ethylenediaminetetraacetic acid (EDTA) [20].

Melamine (MA) is a cheap chemical raw material. There are three free amino groups and three aromatic nitrogen atoms in MA molecule, which is capable of chelating to both Cu(II) and Cu(I) [21–23]. However, as far as we know, CS-based adsorbent using MA as modifier has rarely been reported in references. So, it is expected to obtain inexpensive and high efficient adsorbent by grafting MA onto CS.

Moreover, another important matter is how to separate adsorbents from aqueous solution after adsorption. Traditional separation methods, such as filtration, sedimentation and centrifugation, are both time-consuming and uneconomic [24,25]. Also, if the adsorbents are abandoned with sludge, it will produce secondary pollution. Therefore, it is necessary to choose an effective separation method. Magnetism is a unique physical property of magnetic body and magnetic technology has been used in

* Corresponding authors.
E-mail addresses: wuzhan_chao@163.com (Z.-C. Wu), qustksp@126.com (S.-P. Kuang).

http://dx.doi.org/10.1016/j.ijbiomac.2015.09.020
0141-8130/

separating adsorbents from aqueous solution [26–29]. In this way, a large amount of adsorbent can be separated from aqueous solution in a very short period of time costing less energy and producing no pollutant.

In this work, a new magnetic CS modified by MA (MA-CS/Fe_3O_4) was synthesized successfully. The influences of pH, contact time and initial Cu(II) concentration on adsorption capacity of MA-CS/Fe_3O_4 were studied. The adsorption kinetics and adsorption isotherm were simulated. Also, adsorption and desorption mechanism were discussed.

2. Experimental

2.1. Materials

CS (deacetylation rate >90%) was obtained from Lanji technology development Co., Ltd. (Shanghai, China). Epoxy chloropropane was obtained from Sinopharm Chemical Reagent Co., Ltd. (Shanghai, China). MA and epoxy chloropropane were purchased from Basifu chemical reagent Co., Ltd. (Tianjin, China). Fe_3O_4 with purity of 99.5% and diameter of 20 nm was purchased from Aladdin Chemistry Co., Ltd (Shanghai, China). Solutions of Cu(II) were prepared by dissolving appropriate $Cu(NO_3)_2{\cdot}3H_2O$ (Hongyan chemical reagent factory, Tianjin, China) in deionized water. All other reagents are analytical grade and used without further purification. Deionized water was used in the preparation of all solutions.

2.2. Preparation of MA-CS/Fe_3O_4

CS powders (1.00 g) were dissolved in acetic acid (2 wt.%, 100 mL) and stirred for 2 h. The mixtures were dropped into NaOH (0.25 mol L^{-1}, 100 mL) under stirring. After the precipitation was completed, the mixtures were filtered and the precipitation was washed with acetone. The residues were transferred to acetone (100 mL) and stirred until to suspensions. Epoxy chloropropane (5 mL) was added to above suspensions. Then the mixtures were stirred continuously at 298 K for 24 h. After that, Fe_3O_4 (1.00 g) was added and ultrasonic dispersion was implemented for 20 min. Next, MA (5.50 g) dissolved in DMSO (50 mL) was added and reflux was performed for 7 h at 338 K. Following this, MA (10.00 g) dissolved in DMSO (50 mL), NaOH (1.00 mol L^{-1}, 50 mL) and KI (0.05 g) were added in sequence, and the mixtures were stirred for 5 h. Then the products were cooled, filtered and washed with deionized water and acetone orderly. Finally, the residues were dried in vacuum drying oven at 333 K.

The schematic diagram of synthesis route is shown in Fig. 1.

2.3. Adsorption experiments

Appropriate amounts of MA-CS/Fe_3O_4 were added into Cu(II) solution (200 mol L^{-1}, 20 mL). After adjusting the pH values, the mixtures were shaken in swing bed under the design conditions. Then, the adsorbents were separated from solutions by external magnet. Residual concentration of Cu(II) was measured by flame graphite furnace atomic absorption spectrophotometer (6810F/6810GF). The amounts of Cu(II) adsorbed by per unit mass of adsorbent were obtained by the following equation:

$$Q = \frac{(C_0 - C_e)}{m} V \quad (1)$$

where Q is the adsorption capacity of adsorbent for Cu(II) (mmol g^{-1}); C_0 is the initial concentration of Cu(II) (mmol L^{-1}); C_e is the equilibrium concentrations of Cu(II) (mmol L^{-1}); V and m are the volume of solution (L) and the mass of the dry adsorbent (g).

2.3.1. Effect of pH

Six solution systems with Cu(II) ions (5 mmol L^{-1}) were prepared by adjusting initial pH = 1.0, 2.0, 3.0, 4.0, 5.0 and 5.5. The pH values of the aqueous solutions were measured using pH meter (PHS-25C, Aolilong, Hongzhou). The adsorption experiments were performed by shaking MA-CS/Fe_3O_4 adsorbent (10 mg) with different solution systems (20 mL) at 298 K for 25 min. The residual Cu(II) concentrations in upper clear liquid were detected by flame/graphite furnace atomic absorption spectrophotometer (6810F/6810GF) after separation.

2.3.2. Effect of contact time

The removals of Cu(II) at different time intervals were obtained by shaking MA-CS/Fe_3O_4 adsorbents (10 mg) with Cu(II) solutions (5 mmol L^{-1}, 20 mL, pH = 5.5). Ten parallel experiments were done at 298 K with different adsorption time of 1, 3, 5, 7, 9, 11, 13, 15, 20, 25 and 30 min. The residual Cu(II) concentrations were measured according to the method in Section 2.3.1.

2.3.3. Effect of initial concentration

Ten solution systems (pH = 5.5) with different Cu(II) concentrations were prepared. The initial concentrations of Cu(II) ions were 0.25, 0.5, 1.0, 2.0, 3.0, 4.0, 5.0, 6.0, 7.0 and 8.0 mmol L^{-1}, respectively. The adsorption tests were completed by shaking MA-CS/Fe_3O_4 adsorbents (10 mg) with Cu(II) solution at 298 K for 25 min. The residual Cu(II) concentrations were measured according to the method in Section 2.3.1.

2.4. Desorption and regeneration studies

After adsorption of Cu(II), the adsorbents were collected and washed fully with deionized water in order to remove the unabsorbed metal ions. Then, they were placed into HCl solutions (0.5 mol L^{-1}) and shaken at room temperature for 2 h. After desorption and separation, the adsorbents were still washed with deionized water. The above operations were repeated until no Cu(II) ions were detected in washing liquid. Then they were soaked in NaOH solution (0.5 mol L^{-1}) under stirring for 2 h. After separated from solution, the adsorbents were washed by deionized water and acetone orderly. Finally, they were dried in vacuum drying oven at 333 K. After completing the above steps, the adsorbents were regenerated.

The adsorption and desorption processes were repeated for five times.

2.5. Characterization of the samples

Infrared (IR) spectra were recorded on FT-IR spectrometer (Nicolet 510P, Nicolet, America). X-ray diffraction (XRD) patterns were carried out on X-ray diffractometer (D-MAX 2500/PC, Rigaku, Japan) at voltage of 40 kV and current of 50 mA. The scanning scope of 2θ was from 10° to 80°. The samples morphologies were observed using cold field emission scanning electron microscope (SEM) (JSM-6700F, Hitachi, Japan). The surface area and pore size were measured on micromeritics gas adsorption surface analyzer (ASAP 2020, Micromeritics, America). The content of Fe_3O_4 was determined by thermogravimetric (TG) and differential scanning calorimetric (DSC) analysis using simultaneous thermal analyzer (STA449C, NETZSCH, Germany) under dynamic nitrogen flow at flow velocity of 50 cm^3 min^{-1} and heating rate of 10 K min^{-1}. X-ray photoelectron spectroscopy (XPS) analysis of the adsorbent before and after Cu(II) adsorption was made on a ESCALAB 250 Xi spectrometer (Thermo, America) with an Al Kα X-ray source, operated at 10 mA and 15 kV.

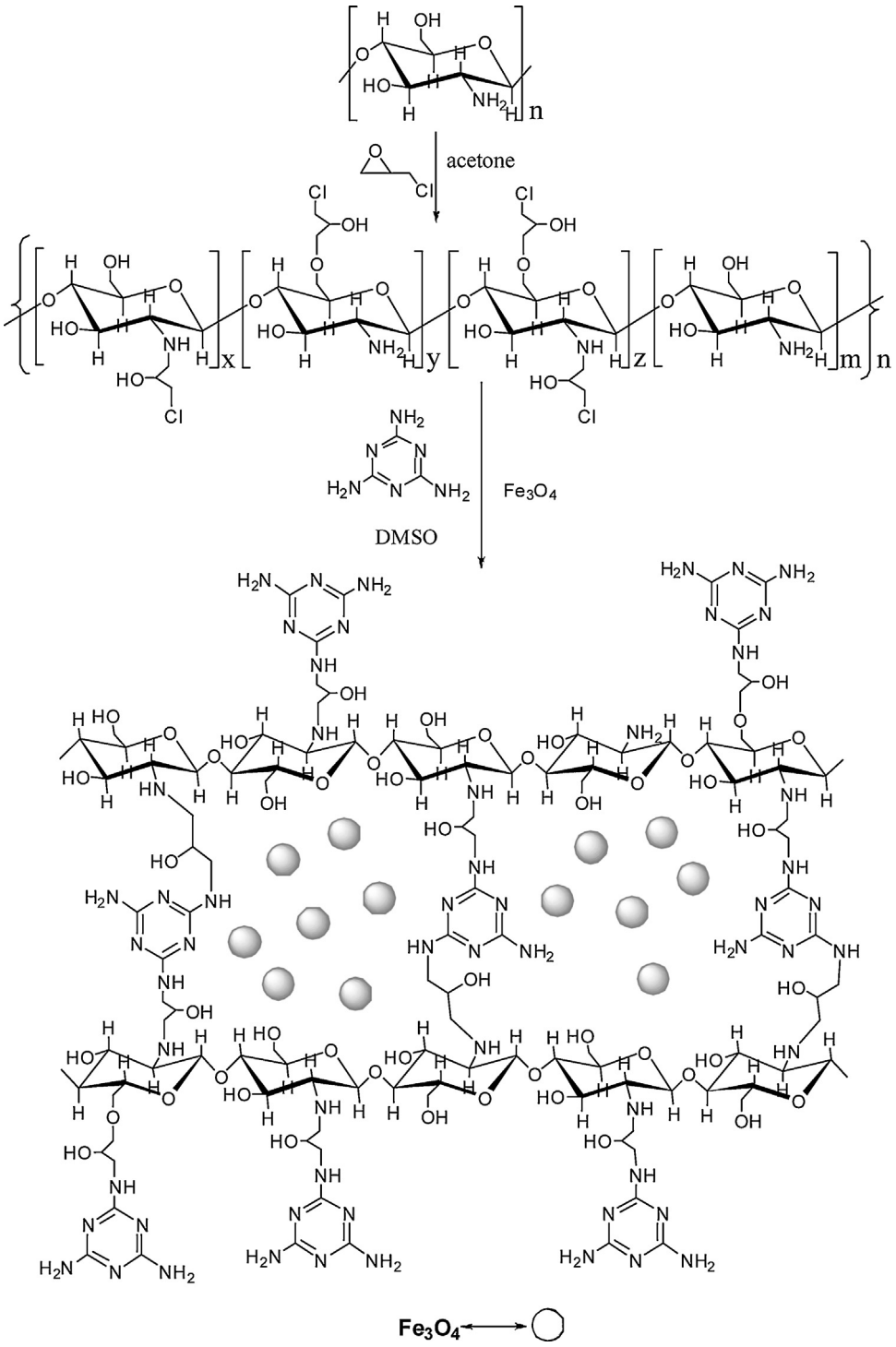

Fig. 1. Synthesis route of MA-CS/Fe_3O_4.

3. Results and discussion

3.1. Charaterization

3.1.1. IR spectra analysis

Fig. 2 shows the IR spectra of CS (curve a), MA (curve c) and MA-CS/Fe_3O_4 (curve b). The molecular formula of MA is $C_3N_6H_6$, in which there are several functional groups including C–N, C=N, NH_2 and triazine ring (see Fig. 1). In general, the peak of N–H stretching vibration is narrower and more cuspate than that of O–H stretching vibration. So the narrow peaks at 3469, 3419, 3335 and 3132 cm^{-1} in curve b and c can be attributed to the stretching vibration of N–H bond in MA [21], while the broad adsorption peaks at 3435 cm^{-1} in curve a is assigned to the stretching vibration of the O–H bond in CS [6]. The spike at 1652 cm^{-1} in curve b and c, which is not observed in curve a, is assigned to the typical bending vibration bands of N–H bond in MA. Whereas the peak at 1637 cm^{-1} in curve a represents the bending vibration of O–H bond in CS. The stretching vibrations of triazine ring correspond to the peaks in the range of 1553–1438 cm^{-1} (see curves b and c) [30]. The twisting vibration

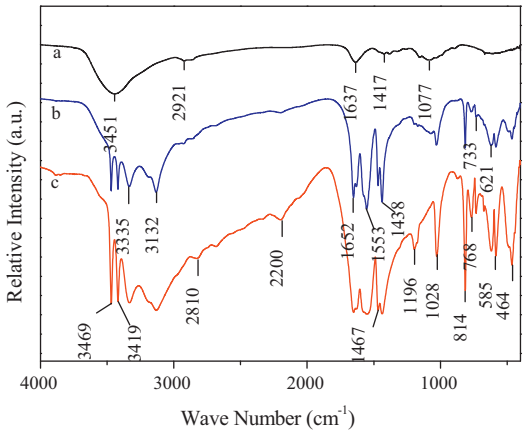

Fig. 2. IR spectra of CS (a), MA-CS/Fe_3O_4 (b) and MA (c).

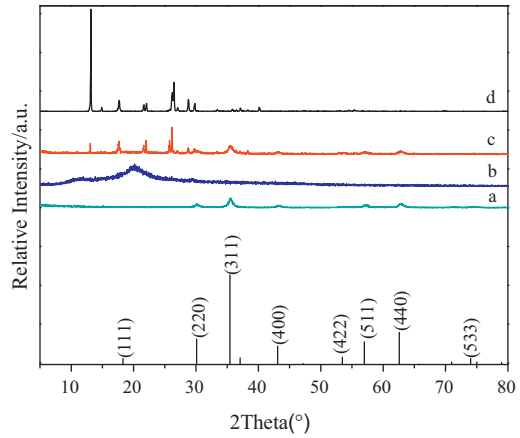

Fig. 3. XRD patterns of Fe_3O_4 (a), CS (b), MA-CS/Fe_3O_4 (c) and MA (d).

of N–H corresponds to the peaks at 1028 cm^{-1} (see curves b and c). The peak at 814 cm^{-1} (in curves b and c) is the characteristic adsorption of triazine ring distorting vibration [30], which is not observed in curve a. Comparisons of the three IR spectra imply that CS was modified by MA successfully.

3.1.2. XRD analysis

Fig. 3 shows the XRD patterns of CS, MA and MA-CS/Fe_3O_4. CS exhibits two very weak characteristic peaks at $2\theta = 10^\circ$ and 20°, respectively. However, they disappear in MA-CS/Fe_3O_4 due to the introduction of epoxy chloropropane, MA and Fe_3O_4, which may change the structure of CS. The diffraction peaks of both Fe_3O_4 ($2\theta = 30.1^\circ$, 35.5°, 43.3°, 57.2° and 62.5°) and MA ($2\theta = 13.2^\circ$, 17.7°, 22.1°, 26.5°, 28.8° and 29.8°) are observed in XRD pattern of MA-CS/Fe_3O_4, while other diffraction peaks of MA ($2\theta = 14.9^\circ$ and 40.1°) disappear in the target product due to the formation of new chemical bonds between MA and CS probably. Meanwhile, the diffraction intensities of MA-CS/Fe_3O_4 become weaker than that of MA, indicating a lower crystallinity of MA-CS/Fe_3O_4 due to the bonding between MA and CS. All the XRD data suggest that MA and Fe_3O_4 have been introduced into CS successfully.

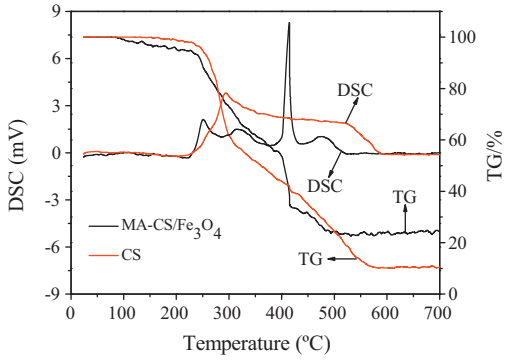

Fig. 5. TG and DSC curve of CS (red line) and MA-CS/Fe_3O_4 (black line). (For interpretation of the references to color in this figure legend, the reader is referred to the web version of this article.)

3.1.3. SEM and BET surface area analysis

The SEM micrographs of the products MA-CS/Fe_3O_4 are given in Fig. 4. It was found that the particles were approximate spherical shape with diameter sizes of about 20–25 nm. Slight agglomerate phenomenon was observed because of the modification. The particles size is nanometer-scale and the surface structure is porous, which make the adsorbents have large specific surface area possibly. The BET specific surface area and pore size of MA-CS/Fe_3O_4 were also determined by nitrogen adsorption measurements. The data of the BET specific surface area and the average pore size were 31.23 $m^2\ g^{-1}$ and 19.63 nm, respectively. Large specific surface area and porous surface structure are favorable to adsorb heavy metal ions.

3.1.4. TG analysis

Fig. 5 reveals the TG and DSC curves of CS (red line) and MA-CS/Fe_3O_4 (black line). The weight loss and enthalpy were 87.90% and 3732.67 $J\ g^{-1}$ for CS decomposition, which started at 493 K and finished at 853 K. Before this stage, it was the water loss process with the weight loss rate about 2.48%. Similarly, the weight loss of MA-CS/Fe_3O_4 was 5.05% between 273 and 493 K due to

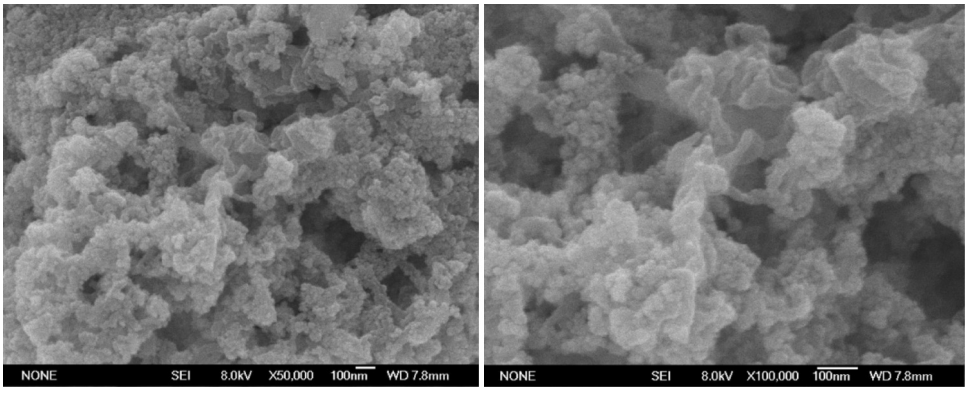

Fig. 4. SEM micrographs of MA-CS/Fe_3O_4.

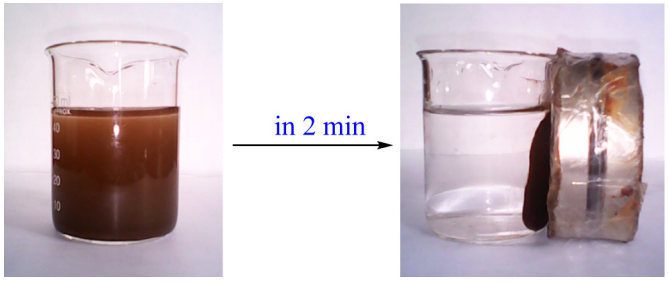

Fig. 6. The separation processes of MA-CS/Fe_3O_4 from their suspensions.

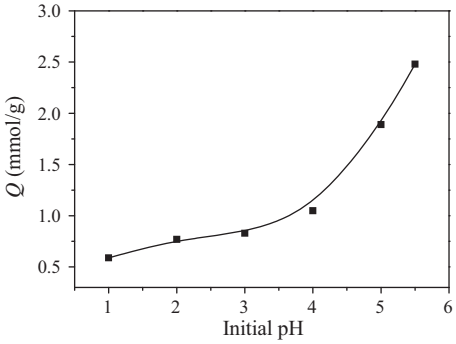

Fig. 7. Effects of initial pH value on adsorption capacity.

the volatilization of water. The organic decomposition step of MA-CS/Fe_3O_4 occurred between 493 and 773 K and the weight loss was 70.90%. 3323.43 J g^{-1} was the enthalpy value of this stage. Fe_3O_4 could not be oxygenated under nitrogen atmosphere. Therefore, the mass content of Fe_3O_4 in MA-CS/Fe_3O_4 is estimated to be about 14.43%.

3.1.5. Magnetic separation performance

Fig. 6 illustrates separation behavior of MA-CS/Fe_3O_4 under magnetic field. The nanometer-scale adsorbent particles were quickly isolated from aqueous solution and transparent liquid was achieved in 2 min, which would bring great convenience in practical applications of the adsorbents.

3.2. Influence of operating conditions on adsorption of Cu(II)

3.2.1. Effects of initial pH

The initial pH of aqueous solution strongly affects the adsorption property of adsorbent. Fig. 7 shows the effects of initial pH value on adsorption capacity of MA-CS/Fe_3O_4. Obviously, the equilibrium adsorption capacity increased with pH value increasing from 1.0 to 5.5, especially when pH values were greater than 4.0. Precipitate was generated in Cu(II) solution (5.0 mmol L^{-1}) when pH value was over 5.5. So, the optimal pH value for Cu(II) adsorption was determined to be 5.5 and the maximum adsorption capacity was 2.48 mmol g^{-1} in this situation. The phenomenon might result from the following facts. MA-CS/Fe_3O_4 contains large amounts of amino, imino and hydroxyl groups. Most of these groups were protonated easily at low pH value, which was unfavorable to adsorb Cu(II) because of electrostatic repulsion. The electron-donating ability of N or O atoms was weakened due to the protonation. These leaded to decrease the adsorption capacity of the adsorbent. With the increase of pH value, the deprotonation was strengthened. Correspondingly, the adsorption capacity of MA-CS/Fe_3O_4 for Cu(II) also increased. Therefore, MA-CS/Fe_3O_4 is more suitable for Cu(II) adsorption at high pH value.

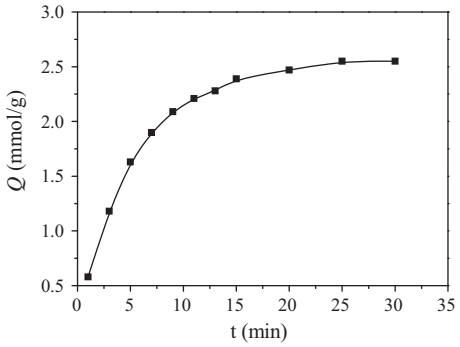

Fig. 8. Effects of contact time on adsorption capacity.

3.2.2. Adsorption kinetics

Fig. 8 shows the effects of contact time on adsorption capacity. The kinetic curve exhibits that the adsorption velocity was rapid at the beginning, and then slowed down gradually. Finally, it was close to adsorption equilibrium at 25 min. So the optimal adsorption time were confirmed to be 25 min.

In order to investigate the adsorption behavior of MA-CS/Fe_3O_4 for Cu(II), pseudo-first-order and pseudo-second-order kinetic models were introduced.

The pseudo-first-order equation [18] is as follows:

$$\frac{1}{Q_t} = \frac{k_1}{Q_e t} + \frac{1}{Q_e} \tag{2}$$

where Q_e and Q_t (mmol g^{-1}) are the adsorption quantities at equilibrium and unequilibrium time (min), respectively; k_1 is the rate constant of pseudo-first-order adsorption (min^{-1}); t is adsorption time. The slope and intercept of the plot of $1/Q_t$ versus $1/t$ are used to determine the first-order rate constant k_1. The slope and intercept are k_1/Q_e and $1/Q_e$, respectively (see Fig. 9(a)).

Another one is pseudo-second-order kinetic model [31]. It is expressed by:

$$\frac{t}{Q_t} = \frac{1}{k_2 Q_e^2} + \frac{t}{Q_e} \tag{3}$$

where k_2 is the equilibrium rate constant of pseudo-second-order adsorption (g $mmol^{-1}$ min^{-1}). The slope and intercept of plotting of t/Q_t versus t are used to calculate the second-order rate constant k_2. The slope and intercept are $1/Q_e$ and $1/k_2 Q_e^2$, respectively (see Fig. 9(b)).

The corresponding kinetic parameters obtained from the above two models were listed in Table 1. The calculated Q_e values are 2.98 and 2.93 mmol g^{-1} according to pseudo-first-order and pseudo-second-order models, respectively. Both calculated Q_e values are close to the experimental Q_e values (2.55 mmol g^{-1}). However, the correlation coefficient (R^2) obtained from the second-order adsorption kinetic model (0.99976) is higher than that from the first-order kinetic model (0.99792), suggesting that the pseudo-second-order equation is more appropriate to simulate the experimental kinetic data [32]. The results indicate that the adsorption rate between MA-CS/Fe_3O_4 and Cu(II) appears to be controlled by the chemical adsorption [33,34].

Most adsorption reactions contain several steps (i) external film diffusion, (ii) intra-particle diffusion and (iii) chemical adsorption. Since the first step is excluded by sufficient shaking the solution, the rate-controlling step is one of the latter two steps. So the data were treated by intra-particle diffusion model [35,36] in order to evaluate the contribution of intra-particle diffusion on rate-controlling step. Its equation is expressed as:

$$Q_t = k_p t^{1/2} + C \tag{4}$$

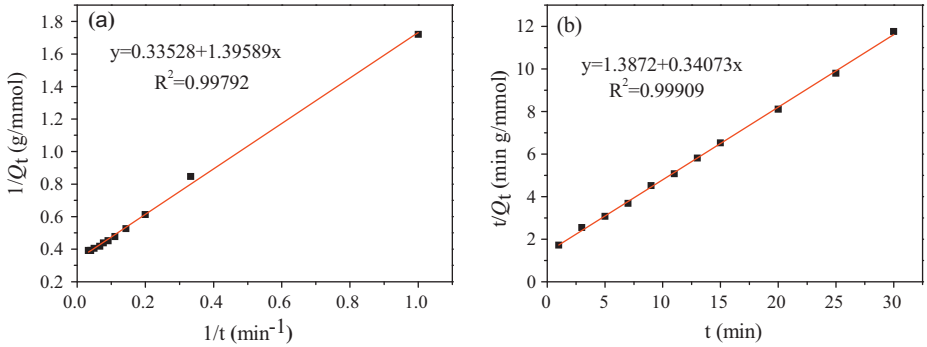

Fig. 9. The adsorption models of first-order kinetics (a) and second-order kinetics (b).

Table 1
Estimated adsorption kinetic parameters for the adsorption of Cu(II) onto MA-CS/Fe_3O_4.

First-order			Second-order			Intraparticle diffusion		
Q_e	K_1	R^2	Q_e	K_2	R^2	K_P	C	R^2
2.98	4.16	0.99792	2.93	0.0837	0.99909	−2.04	2.38	0.8118

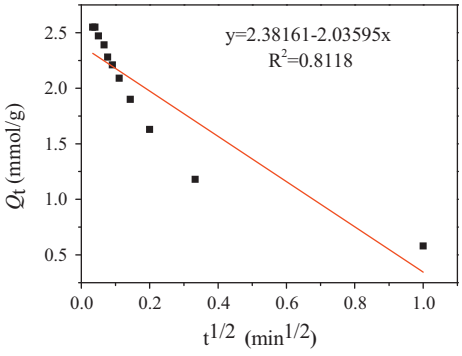

Fig. 10. The intra-particle diffusion model for Cu(II) adsorption by MA-CS/Fe_3O_4.

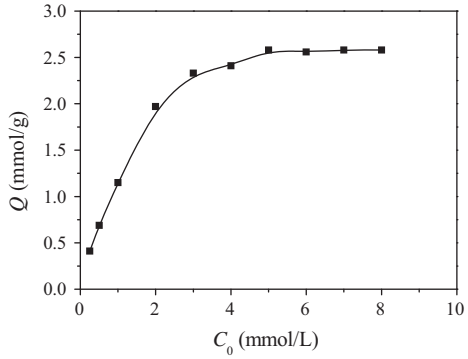

Fig. 11. Effects of initial Cu(II) concentrations on adsorption capacity.

where k_p is the rate constant of the intra-particle diffusion (mmol g^{-1} $min^{1/2}$). The values of k_p and C were calculated via the slope and intercept of the plot of Q_t versus $t^{1/2}$ (see Fig. 10) and the results were also listed in Table 1. It is found the value of R^2 is low (0.8118), indicating the intra-particle diffusion model fits badly with the experimental data. Therefore, the rate-controlling step is not supposed to be intra-particle diffusion, but chemical adsorption. The result is in agreement with the kinetic results reported by Zhou et al. [34].

3.2.3. Equilibrium adsorption isotherms

Fig. 11 shows the effects of initial Cu(II) concentrations on the adsorption capacity. At first, the adsorption capacity increased sharply with the increase of initial Cu(II) concentration. Then, the momentum slowed down. The adsorption capacity achieved maximum at C_0 = 5.0 mmol L^{-1}. After that, it remained unchanged. Finally, the maximum adsorption capacity was determined to be 2.58 mmol g^{-1}. In comparison with raw chitosan and other adsorbents reported in recent years [27,37–42], the adsorbent of MA-CS/Fe_3O_4 prepared in this work showed higher adsorption capacity (shown in Table 2).

In order to study the adsorption behavior between Cu(II) and adsorbent, Freundlich and Langmuir isotherm models were used to simulate the experiment data.

The Freundlich isotherm model predicts that the adsorption process occurs on energetically heterogeneous surfaces and adsorption capacity is related to the concentration of metal ion at equilibrium [43]. The equation of Freundlich isotherm is as follows:

$$\log Q_e = \log K_F + \frac{1}{n} \log C_e \quad (5)$$

where Q_e and C_e are the adsorption capacity (mmol g^{-1}) and the equilibrium concentration of Cu(II) (mmol L^{-1}), respectively; K_F (mmol g^{-1}) and n are Freundlich constant related to adsorption capacity and intensity. The experimental data were plotted as log Q_e versus log C_e (see Fig. 12(a)).

The Langmuir isotherm model assumes that a monolayer adsorption takes place without any interaction between the adsorbed molecules [44]. The Langmuir model can be expressed as:

$$\frac{C_e}{Q_e} = \frac{C_e}{Q_{max}} + \frac{1}{K_L Q_{max}} \quad (6)$$

where Q_{max} is the maximal absorption capacity (mmol g^{-1}) of adsorbent; K_L is Langmuir constant (L $mmol^{-1}$). The experimental data were plotted as C_e/Q_e versus C_e in order to evaluate the values of Q_{max} and K_L (see Fig. 12(b)).

The obtained constants and correlation coefficients values for Freundlich and Langmuir models are given in Table 3. The Langmuir isotherm model fits better to the experimental data than Freundlich model due to the higher correlation coefficients (R^2). The maximum absorption capacity (2.74 mmol g^{-1}) calculated by Langmuir model matches well with the experimental maximum adsorption capacity

Table 2
Comparison of adsorption capacities of different adsorbents for Cu(II) ions.

Adsorbent	Adsorption capacity (mg g^{-1})	Reference
Raw chitosan	80.17	[37]
Magnetic chitosan microspheres	66.70	[38]
Magnetic Cu(II) ion imprinted composite	71.36	[39]
Epichlorohydrin cross-linked xanthate chitosan	30.21	[40]
Xanthate-modified magnetic chitosan	26.3	[41]
Chitosan-modified magnetic Mn ferritenanoparticles	65.1	[27]
S-doped Fe_3O_4@C NPs	54.7	[42]
MA-CS/Fe_3O_4	2.58 mmol g^{-1} = 163.9 mg g^{-1}	This work

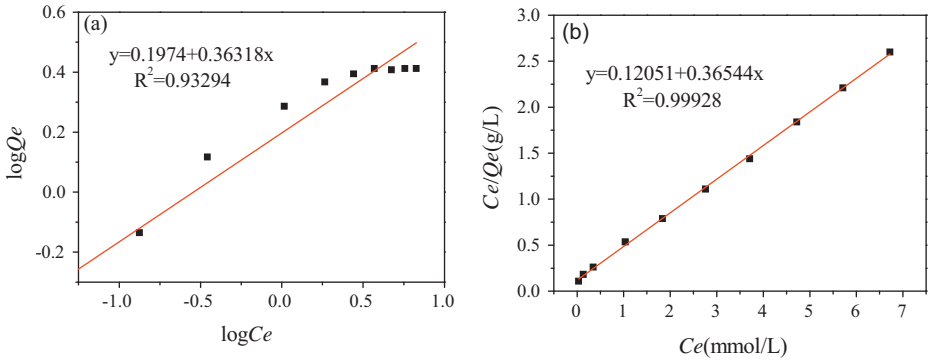

Fig. 12. The Freundlich (a) and Langmuir (b) adsorption isotherms.

Table 3
Simulated adsorption isotherm parameters for the adsorption Cu(II) onto MA-CS/Fe_3O_4.

Freundlich isotherm			Langmuir isotherm		
n	K_F (mmol g^{-1})	R^2	Q_{max} (mmol g^{-1})	K_L (g mmol^{-1})	R^2
2.75	1.58	0.93294	2.74	3.03	0.99928

(2.58 mmol g^{-1}). Based on the above facts, it can be deduced that the monolayer Langmuir adsorption isotherm is more reasonable to explain the adsorption behavior between MA-CS/Fe_3O_4 and Cu(II).

Furthermore, the affinity between the adsorbent and Cu(II) can be predicted by the Langmuir parameter of the dimensionless separation factor R_L, which is defined by the following equation:

$$R_L = \frac{1}{1 + K_L C_0} \quad (7)$$

where C_0 is initial concentration of Cu(II) (mmol L^{-1}); K_L is the affinity constant of Langmuir adsorption (L mmol^{-1}).

The value of R_L is always used to indicate whether the adsorption is favorable or not. $R_L > 1.0$, unfavorable; $R_L = 1.0$, linear; $0 < R_L < 1.0$, suitable and $R_L = 0$, irreversible [45,46]. The values of R_L calculated according to Eq. (7) were listed in Table 4. From Table 4, it can be seen that all of the R_L values are in the range of 0–1.0, indicating that the adsorption of Cu(II) on MA-CS/Fe_3O_4 is favorable.

3.2.4. Regeneration and reuse of MA-CS/Fe_3O_4

Advanced adsorbent is requested to have good regeneration performance as well as excellent adsorption capacity. So the experiments of desorption and reuse were performed through five adsorption–desorption consecutive cycles. As shown in Fig. 13, the regenerative MA-CS/Fe_3O_4 still possessed high adsorption capability, which declined slightly with increasing cycle times. Especially, the value (2.47 mmol g^{-1}) still remained 95.7% of the initial capacity (2.58 mmol g^{-1}) after three cycles. Then the adsorption capacity reduced to 2.05 mmol g^{-1} (about 80% of the initial value) after five times regeneration. Therefore, the adsorbent showed good regenerative performance.

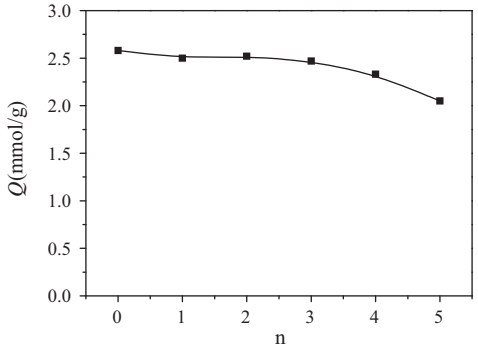

Fig. 13. Effects of regenerative times on the adsorption capacity.

3.3. Adsorption and desorption mechanism

MA-CS/Fe_3O_4 has abundant active groups, such as amino, imino and hydroxyl, which can adsorb Cu(II) by coordination to form Cu(II)-MA-CS/Fe_3O_4 complexes in the surface of adsorbent. The adsorption mechanism of Cu(II) on MA-CS/Fe_3O_4 was investigated by the XPS analysis. Fig. 14 shows typical N 1s XPS spectra of MA-CS/Fe_3O_4 before and after Cu(II) adsorption. Before Cu(II) adsorption, there are only one peak at 398.68 eV, corresponding to the N atoms in the form of –NH_2 and –NH– groups of MA-CS/Fe_3O_4. After the adsorption of Cu(II), the peak of N 1s shifted to 399.48 eV, indicating the formation of –NH_2–Cu(II) or –NH–Cu(II) complexes. In the complexes, a pair of lone electrons from the N atom is shared with the copper ions, and hence the electron cloud density of the N atom is reduced, leading to a higher binding energy (BE) peak [47].

Table 4
The values of separation factor based on the Langmuir equation.

C_0 (mmol L^{-1})	0.25	0.5	1	2	3	4	5	6	7	8
R_L	0.57	0.40	0.25	0.14	0.099	0.076	0.062	0.052	0.045	0.040

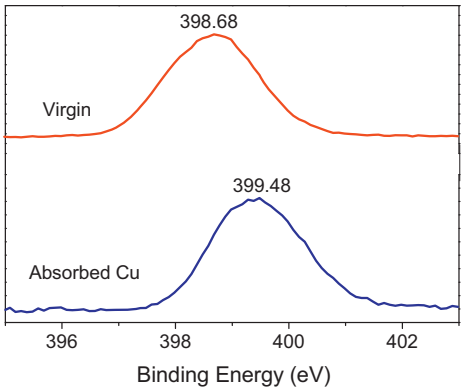

Fig. 14. XPS N 1s spectra of MA-CS/Fe_3O_4 before and after adsorption of Cu(II).

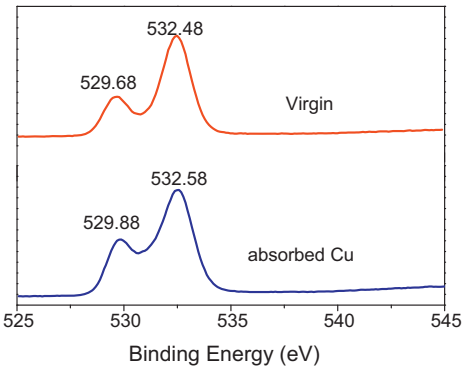

Fig. 15. XPS O 1s spectra of MA-CS/Fe_3O_4 before and after adsorption of Cu(II).

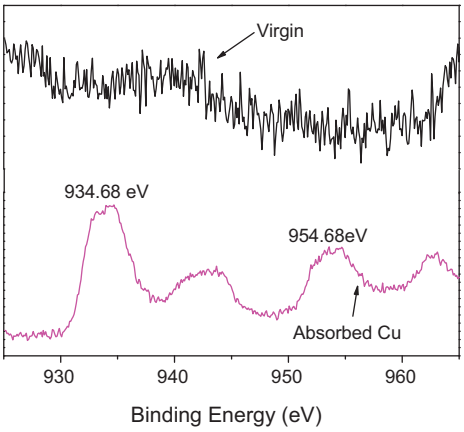

Fig. 16. XPS Cu 2p spectra of MA-CS/Fe_3O_4 before and after adsorption of Cu(II).

The O1s spectra of the adsorbent were investigated, in which the two peaks at 529.68 and 532.48 eV can be assigned to Fe_3O_4 and OH^- groups, respectively [48,49]. After Cu(II) adsorption, the BE values of O1s almost have no change (shown in Fig. 15). This result revealed that the coordination between O atoms of –OH and Cu(II) ions did not occur in the adsorption process.

The XPS Cu 2p spectra of MA-CS/Fe_3O_4 before and after adsorption of Cu(II) are shown in Fig. 16. The XPS spectrum of Cu 2p can be fitted to two peaks at BE of 934.68 (Cu $2p_{3/2}$) and 954.68 eV (Cu $2p_{1/2}$). The peak at BE of 934.68 eV can be assigned to the complexes of $-NH_2$–Cu(II) or –NH–Cu(II), while the peak at BE of 954.68 eV may be attributed to the purely physical Cu(II) adsorption [49]. In addition, the presence of a satellite band nearby the peak at BE of 954.68 eV may represent the oxidation state (+2) of Cu(II) for the Cu $2p_{1/2}$ orbital [50]. The results suggest the accumulation of Cu(II) on the sorbents.

The XPS analysis confirmed that the adsorption process was due to coordination between Cu(II) and N atoms. Nitrogen has a greater tendency to donate its electron pair to Cu(II) to form a complex through a coordinated covalent bond. At the desorption stage, the Cu(II)–MA-CS/Fe_3O_4 complexes were placed into HCl solution, which gave large amounts of H^+. Compared with Cu(II) ions, H^+ ions show stronger coordination ability. So Cu(II) ions were substituted by H^+ ions in Cu(II)–MA-CS/Fe_3O_4 complexes and Cu(II) ions returned to the solution. Finally, the MA-CS/Fe_3O_4 adsorbent was regenerated after being stirred in NaOH solution and washed to neutralize. Therefore, above operations maintained the high adsorption capacity of MA-CS/Fe_3O_4 in each cycle.

4. Conclusions

In this study, a new adsorbent MA-CS/Fe_3O_4 with porous structure was synthesized for removing Cu(II) from aqueous solution. The maximum adsorption capacity was 2.58 mmol g^{-1} at pH = 5.5, T = 298 K, t = 25 min and C_0 = 5.0 mmol L^{-1}. Kinetics study indicates that the adsorption behavior can be better described by the pseudo-second-order equation ($R^2 > 0.999$). Langmuir model fits better with the experimental data ($R^2 > 0.999$), suggesting the monolayer adsorption between the adsorbent and Cu(II). The values of separation constant ($0 < R_L < 1$) indicate that the adsorption for Cu(II) is a favorable process. The rate-controlling step may be chemical adsorption. After adsorbing Cu(II), the Cu(II)–MA-CS/Fe_3O_4 complexes could be rapidly separated from aqueous solution by external magnetic field. The adsorption mechanism was confirmed to be the coordination between Cu(II) and N atoms. The adsorbent possesses excellent regenerative performance. The results show that MA-CS/Fe_3O_4 is a promising adsorbent for removal of Cu(II) from aqueous solutions.

Acknowledgements

This work was financially supported by the National Natural Science Foundation of the People's Republic of China (21007029, 51472132), Qingdao Project of Science and Technology (13-1-4-114-jch), the Natural Science Foundation of Shandong Province (ZR2012BQ017) and the Open Research Program of State Key Laboratory of Geological Processes and Mineral Resources (GPMR201510).

References

[1] L.L. Fan, C.N. Luo, Z. Lv, F.G. Lu, H.M. Qiu, Preparation of magnetic modified chitosan and adsorption of Zn^{2+} from aqueous solutions, Colloids Surf. B: Biointerfaces 88 (2011) 574–581.
[2] L.L. Fan, C.N. Luo, Z. Lv, F.G. Lu, H.M. Qiu, Removal of Ag^+ from water environment using a novel magnetic thiourea-chitosan imprinted Ag^+, J. Hazard. Mater. 194 (2011) 193–201.
[3] J.F. Liu, Z.S. Zhao, G.B. Jiang, Coating Fe_3O_4 magnetic nanoparticles with humic acid for high efficient removal of heavy metals in water, Environ. Sci. Technol. 42 (2008) 6949–6954.
[4] F.L. Mi, S.J. Wu, F.M. Lin, Adsorption of copper(II) ions by a chitosan–oxalate complex biosorbent, Int. J. Biol. Macromol. 72 (2015) 136–144.

[5] L.H. Liu, J. Wu, Y.L. Ling, X. Li, R.J. Zeng, Synthesis of a novel amphoteric chelating polymer flocculant and its performance in Cu^{2+} removal, J. Appl. Polym. Sci. 127 (2013) 2082–2094.
[6] X.Y. Li, H.H. Zhou, W.Q. Wu, S.D. Wei, Y. Xu, Y.F. Kuang, Studies of heavy metal ion adsorption on chitosan/sulfydryl-functionalized graphene oxide composites, J. Colloid Interface Sci. 448 (2015) 389–397.
[7] N.K. Lazaridis, G.Z. Kyzas, A.A. Vassiliou, D.N. Bikiaris, Chitosan derivatives as biosorbents for basic dyes, Langmuir 23 (2007) 7634–7643.
[8] N.V. Majeti, R. Kumar, A Review of chitin and chitosan applications, React. Funct. Polym. 46 (2000) 1–27.
[9] M. Rinaudo, Chitin and chitosan: properties and applications, Prog. Polym. Sci. 31 (2006) 603–632.
[10] H.Q. Bao, L. Li, L.H. Gan, Y. Ping, J. Li, P. Ravi, Thermo- and pH-responsive association behavior of dual hydrophilic graft chitosan terpolymer synthesized via ATRP and click chemistry, Macromolecules 43 (2010) 5679–5687.
[11] F.C. Wu, R.L. Tseng, R.S. Juang, A review and experimental verification of using chitosan and its derivatives as adsorbents for selected heavy metals, J. Environ. Manag. 91 (2010) 798–806.
[12] D.H. Reddy, S.M. Lee, Application of magnetic chitosan composites for the removal of toxic metal and dyes from aqueous solutions, Adv. Colloid Interface Sci. 201–202 (2013) 68–93.
[13] P.A. Nishad, A. Bhaskarapillai, S. Velmurugan, S.V. Narasimhan, Cobalt (II) imprinted chitosan for selective removal of cobalt during nuclear reactor decontamination, Carbohydr. Polym. 87 (2012) 2690–2696.
[14] A. Ghaee, M. Shariaty-Niassar, J. Barzin, A. Zarghan, Adsorption of copper and nickel ions on macroporous chitosan membrane: equilibrium study, Appl. Surf. Sci. 258 (2012) 7732–7743.
[15] S.P. Kuang, Z.Z. Wang, J. Liu, Z.C. Wu, Preparation of triethylene-tetramine grafted magnetic chitosan for adsorption of Pb(II) ion from aqueous solutions, J. Hazard. Mater. 260 (2013) 210–219.
[16] X.J. Hua, J.S. Wang, Y.G. Liu, et al., Adsorption of chromium (VI) by ethylenediamine modified cross-linked magnetic chitosan resin: isotherms, kinetics and thermodynamics, J. Hazard. Mater. 185 (1) (2011) 306–314.
[17] L. Wang, R.G. Xing, S. Liu, Y.K. Qin, K.C. Li, H.H. Yu, R.F. Li, P.C. Li, Studies on adsorption behavior of Pb(II) onto a thiourea-modified chitosan resin with Pb(II) as template, Carbohydr. Polym. 81 (2010) 305–310.
[18] L.M. Zhou, J.H. Liu, Z.R. Liu, Adsorption of platinum(IV) and palladium(II) from aqueous solution by thiourea-modified chitosan microspheres, J. Hazard. Mater. 172 (2009) 439–446.
[19] Y.Z. Wen, J.Q. Ma, J. Chen, C.S. Shen, H. Li, Q.P. Liu, Carbonaceous sulfur-containing chitosan-Fe(III): a novel adsorbent for efficient removal of copper (II) from water, Chem. Eng. J. 259 (2015) 372–380.
[20] Y. Ren, H.A. Abbood, F.B. He, H. Peng, K.X. Huang, Magnetic EDTA-modified chitosan/SiO_2/Fe_3O_4 adsorbent: preparation, characterization, and application in heavy metal adsorption, Chem. Eng. J. 226 (2013) 300–311.
[21] A.B. Wiles, D. Bozzuto, C.L. Cahill, R.D. Pike, Copper (I) and (II) complexes of melamine, Polyhedron 25 (2006) 776–782.
[22] L.F. Xu, X.L. Chen, H.M. Hu, B.C. Wang, Syntheses, structures and electrochemical properties of two co-crystal copper(II) melamine complexes, J. Mol. Struct. 892 (2008) 163–167.
[23] Y. Zhang, K. Chen, H.T. Fan, Synthesis, crystal structure and catalytic property of a new Cu(I) coordination polymer constructed from melamine and azide ligands, Inorg. Chem. Commun. 38 (2013) 47–49.
[24] M. Monier, Adsorption of Hg^{2+}, Cu^{2+} and Zn^{2+} ions from aqueous solution using formaldehyde cross-linked modified chitosan-thioglyceraldehyde Schiff's base, Int. J. Biol. Macromol. 50 (2012) 773–781.
[25] A.W. Chen, G.M. Zeng, G.Q. Chen, X.J. Hu, M. Yan, S. Guan, C. Shang, L.H. Lu, Z.J. Zou, G.X. Xie, Novel thiourea-modified magnetic ion-imprinted chitosan/TiO_2 composite for simultaneous removal of cadmium and 2,4-dichlorophenol, Chem. Eng. J. 191 (2012) 85–94.
[26] L.M. Cui, L.H. Hu, X.Y. Guo, Y.K. Zhang, Y.G. Wang, Q. Wei, B. Du, Kinetic, isotherm and thermodynamic investigations of Cu^{2+} adsorption onto magnesium hydroxyapatite/ferroferric oxide nano-composites with easy magnetic separation assistance, J. Mol. Liq. 198 (2014) 157–163.
[27] Y.Y. Meng, D.Y. Chen, Y.T. Sun, D.L. Jiao, D.C. Zeng, Z.W. Liu, Adsorption of Cu^{2+} ions using chitosan-modified magnetic Mn ferrite nanoparticles synthesized by microwave-assisted hydrothermal method, Appl. Surf. Sci. 324 (2015) 745–750.
[28] D. Hritcu, M.I. Popa, N. Popa, V. Badescu, V. Balan, Preparation and characterization of magnetic chitosan nanospheres, Turk. J. Chem. 33 (2009) 785–796.
[29] H. Yan, L.Y. Yang, Z. Yang, H. Yang, A.M. Li, R.S. Cheng, Preparation of chitosan/poly(acrylic acid) magnetic composite microspheres and applications in the removal of copper(II) ions from aqueous solutions, J. Hazard. Mater. 229–230 (2012) 371–380.
[30] G.Y. Tian, C.B. Lu, H.F. Yuan, Determination of melamine concentration in milk powder and liquid milk by Fourier transform-infrared spectroscopy, Mod. Sci. Instr. (China) (5) (2009) 86–91.
[31] L.L. Li, C.N. Luo, X.J. Li, H.M. Duan, X.J. Wang, Preparation of magnetic ionic liquid/chitosan/graphene oxide composite and application for water treatment, Int. J. Biol. Macromol. 66 (2014) 172–178.
[32] L.L. Fan, C.N. Luo, M. Sun, X.J. Li, H.M. Qiu, Highly selective adsorption of lead ions by water-dispersible magnetic chitosan/graphene oxide composites, Colloids Surf. B 103 (2013) 523–529.
[33] M. Monier, D.M. Ayad, Y. Wei, A.A. Sarhan, Adsorption of Cu(II), Co(II), and Ni(II) ions by modified magnetic chitosan chelating resin, J. Hazard. Mater. 177 (2010) 962–970.
[34] L.M. Zhou, C. Shang, Z.R. Liu, G.L. Huang, A.A. Adesina, Selective adsorption of uranium(VI) from aqueous solutions using the ion-imprinted magnetic chitosan resins, J. Colloid Interface Sci. 366 (2012) 165–172.
[35] K.Z. Elwakeel, A.A. Atia, Uptake of U(VI) from aqueous media by magnetic Schiff's basechitosan composite, J. Clean. Prod. 70 (2014) 292–302.
[36] A.A. Atia, A.M. Donia, K.Z. Elwakeel, Recovery of gold(III) and silver(I) on a chemically modified chitosan with magnetic properties, Hydrometallurgy 87 (2007) 197–206.
[37] W.S.W. Ngah, C.S. Endud, R. Mayanar, Removal of copper(II) ions from aqueous solution onto chitosan and cross-linked chitosan beads, React. Funct. Polym. 50 (2002) 181–190.
[38] L.M. Zhou, Y.P. Wang, Z.R. Liu, Q.W. Huang, Characteristics of equilibrium, kinetics studies for adsorption of Hg(II), Cu(II), and Ni(II) ions by thiourea-modified magnetic chitosan microspheres, J. Hazard. Mater. 161 (2009) 995–1002.
[39] Y.M. Ren, M.L. Zhang, D. Zhao, Synthesis and properties of magnetic Cu(II) ion imprinted composite adsorbent for selective removal of copper, Desalination 228 (2008) 135.
[40] B. Kannamba, K.L. Reddy, B.V. AppaRao, Removal of Cu(II) from aqueous solutions using chemically modified chitosan, J. Hazard. Mater. 175 (2010) 939–948.
[41] Y.H. Zhu, J. Hu, J.L. Wang, Competitive adsorption of Pb(II), Cu(II) and Zn(II) onto xanthate-modified magnetic chitosan, J. Hazard. Mater. 221–222 (2012) 155–161.
[42] L.Q. Zhao, X.L. Chang, R. Liao, X.L. Zhang, J.R. Xie, B.W. Yu, R.H. Wu, R.J. Wang, S.T. Yang, Facile hydrothermal preparation of S-doped Fe_3O_4@C nanoparticles for Cu^{2+} removal, Mater. Lett. 135 (2014) 154–157.
[43] Z. Zawani, C.A. Luqman, S.Y.C. Thomas, Equilibrium, kinetics and thermodynamic studies: adsorption of Remazol Black 5 on the palm kernel shell activated carbon (PKS-AC), Eur. J. Sci. Res. 37 (2009) 63–71.
[44] Y.H. Li, Z. Di, J. Ding, D. Wu, Z. Luan, Y. Zhu, Adsorption thermodynamic, kinetic and desorption studies of Pb^{2+} on carbon nanotubes, Water Res. 39 (2005) 605–609.
[45] Z. Aksu, Determination of the equilibrium, kinetic and thermodynamic parameters of the batch biosorption of nickel (II) ions onto *Chlorella vulgaris*, Process Biochem. 38 (2002) 89–99.
[46] A.S. Alzaydien, W. Manasreh, Equilibrium, kinetic and thermodynamic studies on the adsorption of phenol onto activated phosphate rock, Int. J. Phys. Sci. 4 (2009) 172–181.
[47] C.X. Liu, R.B. Bai, Adsorptive removal of copper ions with highly porous chitosan/cellulose acetate blend hollow fiber membranes, Membr. Sci. 284 (2006) 313–322.
[48] D. Wilson, M.A. Langell, XPS analysis of oleylamine/oleic acid capped Fe_3O_4 nanoparticles as a function of temperature, Appl. Surf. Sci. 303 (2014) 6–13.
[49] F. Yang, H.J. Liu, J.H. Qu, J.P. Chen, Preparation and characterization of chitosan encapsulated *Sargassum* sp. biosorbent for nickel ions sorption, Bioresour. Technol. 102 (2011) 2821–2828.
[50] W. Jiang, X.B. Chen, B.C. Pan, Q.X. Zhang, L. Teng, Y.F. Chen, L. Liu, Spherical polystyrene-supported chitosan thin film of fast kinetics and high capacity for copper removal, J. Hazard. Mater. 276 (2014) 295–301.